Degradation and Characterisation of Resorbable Phosphate-Based Glass Thin Film Coatings Applied by RF magnetron Sputtering

Bryan Stuart*, Miquel Gimeno-Fabra, Joel Segal, Ifty Ahmed, David M. Grant*

Department of Mechanical, Materials and Manufacturing Engineering, University of Nottingham, epxbs4@nottingham.ac.uk, david.grant@nottingham.ac.uk

Keywords

Phosphate glass, Bioresorbable, Bioactive Thin Films, Osseointegration, Dissolution, Sputtering, PVD

Abstract

Quinternary phosphate based glasses of up to 2.67 μm, deposited by RF magnetron sputtering were degraded in distilled water and phosphate buffer saline to investigate their degradation characteristics. Magnetron sputtered coatings have been structurally compared to their compositionally equivalent melt quenched bulk glass counterparts. The coatings were found to have structurally variable surfaces to melt quenched glass such that the respective bridging oxygen to non-bridging oxygen bonds on the surface were 34.2% : 65.2% vs. 20.5% : 78.5 % forming metaphosphate $(PO_3)^-$ (Q^2) vs. less soluble $(P_2O_7)^{4-}$ (Q^1) and $(PO_4)^{3-}$ (Q^0) respectively. This factor led to highly soluble coatings, exhibiting a $t^{1/2}$ degradation dependence in the first 2 hours in distilled water, followed by a more characteristic linear profile as the subsequent layers were less soluble. Hydration and degradation was observed to preferentially occur, forming voids characteristic of pitting corrosion which was confirmed by use of a Focused Ion Beam. Coating degradation in PBS precipitated a $(PO_3)^-$ metaphosphate, X-Ray amorphous layer, which remained adherent to the substrate and seemingly formed a protective diffusion barrier which inhibited further coating degradation. The implications are that whilst compositionally similar, sputter deposited coatings and melt quenched glasses are structurally dissimilar, most notably, with regards to the surface layer. This factor has been attributed to surface etching of the as deposited coating layer during

deposition and variation in the thermal history between the processes of magnetron sputtering and melt quenching.

1. Introduction

Resorbable phosphate based glasses (PBG) can be tailored to deliver ions during dissolution [1-3] and this distinct advantage could potentially be extended to the production of thin film coatings for orthopaedic implants [4-9]. PBG compositions such as the P_2O_5-40 MgO-24 CaO-16 Na_2O-16 Fe_2O_3-4 mol% [10] have demonstrated cytocompatibility whilst others such as P_2O_5-30 CaO-60 Na_2O-7 TiO_2-3 mol% [11] have exhibited bioactive behaviour *in vitro*, similar to the well-known commercially available 45S5 Bioglass® [11-13].

Kim *et al* produced PBG/hydroxyapatite (HA) composite coatings of 30-40 μm via a sol gel method, with a phosphate glass/HA porous slurry on commercially pure titanium, subsequently densified by an HA sol gel precursor. The coatings demonstrated a favourable cellular response towards human osteoblast cells *in vitro* over the titanium control [14]. Sol gel coatings are known to suffer from poor adhesion whilst the commercially popular method of plasma spraying HA can generate relatively thick structures in the order of 10's to 100's of microns which are not single phase and contain porosity and cracks which can lead to inferior adhesion [14-15].

As shown by Lo *et al*, Radio frequency (RF) magnetron sputtering has proven to be a useful technique for the controlled deposition of dense uniform thin films of controlled crystallinity of HA and single and mixed phases of CaP based targets [16-19]. In addition a number of bioactive silicate glass compositions have been sputtered, including the composition deposited by Stan and Berbecaru *et al* SiO_2-40.5 CaO-32 P_2O_5-1.5 Na_2O-9 MgO-17 mol% which showed the formation of apatite *in vitro* following submersion in Simulated Body Fluid (SBF) [20-25]. The controlled natural formation of HA from the dissolution of bioactive

glass may allow for customised rates of HA and ion release rates necessary for specific bone defects. Mistry *et al* showed that bioactive glass outperformed synthetic HA compositions with respect to bone apposition *in vivo* [26]. Notably, bioglass 45S5 is specifically effective in its ability to bond to soft tissues [27] [12]. Recently, the controlled deposition of quaternary and quinternary phosphate based glass compositions by RF magnetron sputtering has been demonstrated via manipulation of the coating parameters [28].

Degradation studies on PBGs have frequently been conducted using deionised water and distilled water (dH_2O) [4, 7, 29-31]. In addition, *In vitro* media such as SBF, Simulated Urine (SU), and Phosphate Buffered Saline (PBS) have also been used as dissolution media [32-33]. SBF and SU mimic ionic concentration and chemical compositions of human blood plasma and urine respectively whilst PBS is one of many saline solutions which function as a buffering solution to recreate the pH conditions within the body as the solution buffers to a pH of 7.40 [4-5] [32-34]. Bunker *et al* showed degradation of bulk phosphate glasses to be highly pH dependent, with increased degradation at lower pH [30].

The degradation mechanisms of PBGs has been shown to vary based on changes in glass compositions [1, 3, 29-30]. Phosphate-based glasses degrade in aqueous solution by reacting with H_2O molecules to break the P-O-P bonds and depolymerise the network [30-31]. The process has been described to occur in three stages for glass containing monovalent cations such as sodium. First, the acid/base reaction during which the glass surface becomes saturated with acid H^+ or base OH^- ions, linearly increasing in time until no more uptake is possible [30-31]. Secondly, H_2O molecules hydrate the network by diffusion showing an exponential degradation profile of $t^{1/2}$ [30]. Bunker *et al* described the third linear dissolution phase as a hydrolysis reaction where the polymeric phosphate chains began to disentangle and separate completely via hydrolytic attack [30].

Bunker *et al* also showed that ternary phosphate based glasses doped with alkali ions of sodium, lithium or potassium showed a reduction in durability with increasing alkali content such that elements with greater atomic radii added in the same proportions degraded faster. The range of dissolution based on compositions of 50-P_2O_5 (50-X)-M_2O (X)-CaO varied from 10^{-4} to 10^{-9} g $cm^{-2}min^{-1}$ [30]. This range of degradation characteristics demonstrates the flexibility associated with optimisation of PBG formulations and their dissolution rates and products.

The aim of this study was to assess and compare the degradation of thin film PBGs coatings on Ti6Al4V substrates in both PBS and dH_2O to assess the potential development of a resorbable PBG layer, with the potential to release ions at the implant site.

2. Materials and Methods

2.1 Target Preparation

Pre-calculated (mol%) proportions of precursor salts namely sodium dihydrogen phosphate (NaH_2PO_4), calcium hydrogen phosphate ($CaHPO_4$), magnesium phosphate dibasic trihydrate ($MgHPO_43H_2O$), Iron phosphate dehydrate ($FePO_42H_2O$) and phosphorous pentoxide (P_2O_5) (Sigma Aldrich, U.K.), were thoroughly mixed then preheated at 400 °C to dehydrate. The mixture was then melted at 1200 °C for 2 h in air. The targets were formed by quenching the molten mixture at 450 °C followed by slow cooling at 5 °C min^{-1} to room temperature. The target mould and the subsequent target measured 75 ± 2 mm in diameter and 6 ± 1 mm in thickness. See *Table 1* for target compositions produced.

2.2 X-Ray Diffraction

Samples of the glass targets were ground to a fine powder for X-Ray diffraction (XRD) analysis (Bruker D8, Cu Kα source: λ=1.5418 Å, 40 kV, 40 mA) conducted over a 2θ range

from 15° to 65° with a step size of 0.04° in 2θ, and a dwell time of 5 s. In addition glancing angle XRD was performed on the deposited coatings utilising a step size of 0.02° in 2θ.

2.3 Fourier Transform Infrared Spectroscopy

A Bruker Tensor Fourier Transform Infrared Spectrometer (FTIR) with an Attenuated Total Reflectance (ATR) attachment was used for all Infrared absorption measurements of the as-prepared coated samples. A spectral resolution of 4 cm^{-1} over the wavenumber range 500-4000 cm^{-1} was set. All spectra obtained represent the average of 64 scans over the sample area. The IR spectra were processed and analysed using the OPUS spectroscopy software.

2.4 Energy Dispersive X-Ray Spectroscopy

The compositions of the sputtering targets and sputtered coatings were determined via a Phillips XL30 SEM-EDX. Energy Dispersive X-Ray Spectroscopy (EDX) was conducted at a working distance of 10 mm at a minimum of 200,000 counts and a beam voltage of 15 kV. The X-Ray beam current was optimised by increasing the spot size to obtain a minimum acquisition rate of 4,000 counts/sec whilst maintaining an acquisition dead time <30%. The glass compositions detailed in tables 1 and 2 are with respect to the oxidative states in the glasses as commonly reported for phosphate glass structures [1,3,5,6].

2.5 Scanning Electron Microscopy

The coating cross sections and surface images were obtained via Scanning Electron Microscopy (SEM) using a Phillips XL30-ESEM. The working distance was kept constant at 10 mm, utilising a beam voltage of 20 kV.

2.6 Focussed Ion Beam Scanning Electron Microscope

The coatings on Ti6Al4V substrates were sectioned and polished via a Focussed Ion Beam (FIB) using a Zeiss NVision 40 with a gallium milling source. The working distance was kept

constant at 5 mm utilising a beam voltage of 5.00 kV. All sections were cut at a tilt angle of 54°.

2.7 X-Ray Photoelectron Spectroscopy

X-Ray Photoelectron Spectroscopy (XPS) was conducted using a VG Scientific EscaLab Mark II with an Al kα non-monocromatic X-Ray source. Scans were collected at 20 mA and 12 kV emissions.

2.8 Sample Preparation for Coating Deposition

Substrates for coating were 1.5 mm thick, 10 mm diameter Ti6Al4V (grade 5) discs wire eroded from sheet. The discs were wet polished to a 6 μm finish using silicon carbide paper from grades P200-P4000 and further polished on a 0.25 μm chemomet finishing pad with the application of colloidal silica. The polished substrate roughness was measured as 0.114 ± 0.013 μm (SD) (n=10) using a 3D Interferometer (Fogale Photomap 3D). Roughened samples were sandblasted with 220P alumina sand particles at a distance of 50 ± 5 mm and an air pressure of 7 x 10^5 Pa. The roughness was measured as 0.788 ± 0.061 (SD) (n=10). All measurements were collected over a scan area of 800 μm^2. Samples were then ultrasonically cleaned for 10 min in acetone, followed by distilled water. 100 μm thick borosilicate cover slides were also coated to measure the coating thicknesses achieved. Prior to coating, the slides were platinum coated for 90 s at 1.2 keV in a Polaron sputter coater to enhance the interfacial contrast between coating and glass for microscopy analysis. The sides of the samples discs (lateral surfaces) were masked with a polyimide film to restrict deposition to the plane parallel to the magnetron.

2.9 Degradation of Bulk Glass Target Compositions

Glass rods were produced following the procedure in section 2.1 and subsequently quenched in 9 mm diameter graphite moulds to form rods. The rods were cut into 5 mm cylinders using

a diamond saw. Three cylinders were placed into separate containers of 30 ml of phosphate buffer solution pH ≈ 7.40 and incubated at 37 °C. The cylinders were left in solution for 2, 4, 8, 12, 16 and 24 h followed by 2, 3, 5, 8, 12, 16, and 20 days, then every 7 days until 83 days. At each time point the cylinders were removed, dried with tissue and placed in an oven at 50 °C for 1 h to remove excess surface water. The surface area and mass were measured using a Vernier calliper and a Mettler Toledo precision scale accurate to 0.01 mg. The samples were then re-submerged until the next measurement time point. The PBS and distilled water were changed at each time point until 7 days then subsequently twice per week. The pH was measured before and after degradation at room temperature when using PBS. The pH was measured after degradation when using distilled water. Pre prepared tablets of PBS from Sigma Aldrich were dissolved in 200 mL of distilled water.

2.10 Degradation of Coatings

The phosphate glass compositions C1: P28 and C2: P40 were applied to both polished and sandblasted Ti6Al4V (Grade 5) substrates by RF magnetron sputtering.

For SEM analysis the coated discs were submerged in 15 mL of solution (PBS or dH_2O) and incubated at 37 ± 2 °C. 3 isolated coated samples were observed at each time point. The solution was not changed over the test period. Separate samples of each time point were utilised to prevent from disturbing the coating layer. The pH was measured pre and post degradation to ensure the solution did not become saturated. Samples could not be re-submerged following conductive coating for imaging due to contamination inhibiting degradation.

Mass loss per unit surface area data was recorded for coatings on sandblasted substrates, as bulk coating lift off or delamination had been observed on polished substrates. All samples were weighed prior to deposition and post deposition to determine the mass of the coatings.

Samples were subsequently submerged in 15 mL of solution and incubated at 37 ± 2 °C (n =3). For all data points beyond 24 h, the 24 h samples were re-submerged. At each time point the discs were removed, and placed in an oven at 50 °C for 1 h to remove surface moisture.

2.11 Contact Angle

The contact angle was assessed utilising dH_2O (pH≈7.0). A polar liquid was chosen due to the hydration interacting with phosphate glasses. dH_2O was pumped out at a rate of 1.0 μl/s and dropped at a height of 4.0 ± 0.5 mm. The drop was allowed to settle for 10 s prior to collecting results. For each sample type (n=5).

2.12 Coating Deposition

The coatings were deposited via a custom in-house designed Physical Vapour Deposition (PVD) utilizing a RF (13.56 MHz) magnetron sputtering rig, with a phosphate glass target T1 of composition detailed in Table 1. The chamber was pumped down to a vacuum utilising a combination of a rotary (Edwards E2M-18) and turbo molecular pump (Edwards EXT250) to a base pressure <7 x 10^{-3} Pa. Phosphate glass deposition was performed at pressures of 10 ± 0.05 and 2.2 ± 0.05 mTorr Pa in 99.99% pure shield argon at 60 ± 1 W deposition power or the equivalent of 13.6 kW m^{-2}. The distance between target and substrate was also held constant at 4 ± 0.5 cm. Prior to deposition, targets were sputter cleaned for 30 min at 30 W and then increased to 60 W for a further 30 min. The deposition parameters and sample nomenclature are listed in *Tables 2* and *3*. Target glass has been labelled (T), Bulk glass rods as (B) and coatings as (C). Nominal compositions have been denoted by (N) whilst as prepared compositions have been denoted by (AP). (AP) compositions were assessed via EDX compositional analysis (*Tables 2* and *3).*

Table 1: Nominal and As Prepared Targets, Coatings and Melt Quenched Rods for Deposition and Degradation.

Glass Code Nominal (N) vs. As Prepared (AP)	P_2O_5	MgO	CaO	Na_2O	Fe_2O_3
T1 (N)	51.50	18.50	14.00	11.00	5.00
T1 (AP)	49.81 ± 0.11	19.31 ± 0.08	13.31 ± 0.09	13.15 ± 0.11	4.42 ± 0.53

Table 2: Coating Deposition Parameters

Deposition Parameters	Argon Pressure (mTorr)	Deposition Time (min)	Power (W)	Throw Distance (cm)	Rotation (RPM)	Coating Thickness (μm)
C1	2.20 ± 0.1	1165 ± 1	60 ± 1	4.0 ± 0.5	Static	1.69 ± 0.01
C2	10.0 ± 0.1	1165 ± 1	60 ± 1	4.0 ± 0.5	Static	2.69 ± 0.09

Table 3: As Prepared Coating and Rod Compositions.

Glass Code Nominal (N) vs. As Prepared (AP)	P_2O_5	MgO	CaO	Na_2O	Fe_2O_3
C1/ B1: P28 (N)	28	27	20	19	6
C2/ B2: P40 (N)	40	24	16	16	4
C1: P28 (AP)	27.77 ± 0.15	27.3 ± 0.23	20.41 ± 0.07	18.97 ± 0.16	6 ± 0.08
C2: P40 (AP)	40.23 ± 0.19	23.83 ± 0.15	15.37 ± 0.15	16.75 ± 0.14	3.82 ± 0.53
B1: P28 (AP)	28.34 ± 0.09	24.63 ± 0.11	20.56 ± 0.08	20.81 ± 0.16	5.67 ± 0.07
B2: P40 (AP)	39.64 ± 0.08	24.49 ± 0.08	15.59 ± 0.07	16.73 ± 0.06	3.55 ± 0.06

3. Results

3.1 X-Ray Diffraction for Deposited Coatings, Melt Quenched Targets and Bulk Rods

Bulk melt quenched glass target (T1: P51.5) and glass rod (B2: P40) were confirmed to be amorphous via XRD analysis *(see Figure 1A).* However, the melt quenched rod (B1: P28) was found to be crystalline *(see Figure 1A).* The deposited coating C2: P40 was also confirmed to be amorphous; however, a crystalline phase corresponding to FeOOH was found in C1: P28. The phases attributed to the substrate Ti6Al4V and Al_2O_3 from sample preparation were also found to be present (see *Figure 1B*).

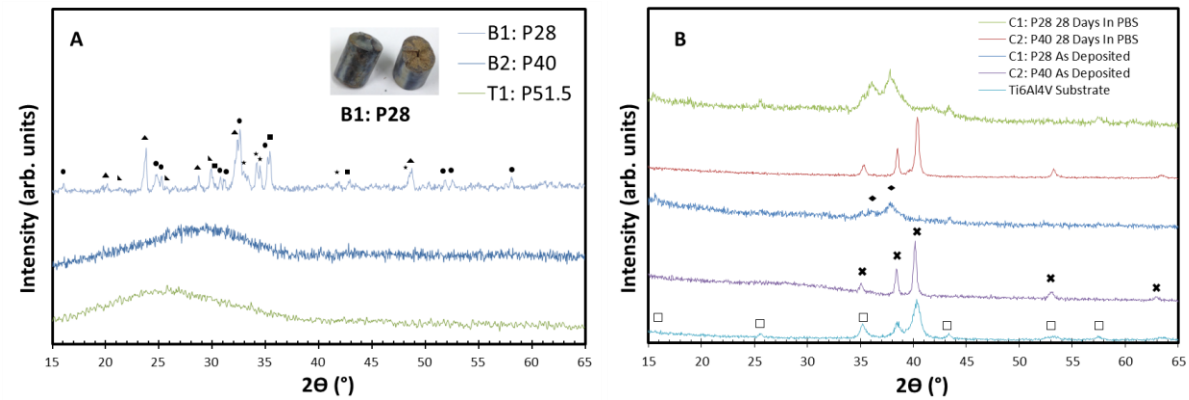

Figure 1: (A) XRD of amorphous T1, B1 and B2. Crystalline rod B1 phases corresponding to (★) Brianite $Na_2CaMg(PO_4)_2$ ICDD-PDF-01-088-1549 (▲)Sodium Iron Phosphate $Na_3Fe_2(PO_4)_3$ ICDD-PDF-00-045-0319 (■)Magnetite Fe_3O_4 ICDD- PDF-01-075-1610 (◣)Magnesium Phosphate Oxide $Mg_2P_2O_7$ ICDD-PDF-01-075-1610 (●) Main peaks attributed to unidentified phases (B) XRD of coatings C1, and C2 as deposited and 28 days post degradation of C1: P28 and C2: P40 in PBS. Crystalline phases corresponding to (□) Aluminium Oxide Al_2O_3 ICDD-PDF-00-081-1667 (◆) Lepidocrocite FeOOH ICDD-PDF-01-076-2301 (×) Titanium ICDD PDF-00-001-1197.

X-Ray diffraction for as deposited coatings suggested no additional crystalline structures for coatings C1 and C2, 28 days post submersion in PBS as shown in *Figure 1B.*

3.2 Degradation of Bulk Glass in PBS and dH_2O

The bulk glass rod composition B2: P40 exhibited a linear degradation profile over the 83 day test period in both PBS and dH_2O (see *Figure 2B*). Based on the slope of the degradation, dissolution occurred at a rate of 1.38 times faster in dH_2O than PBS for B2: P40 over the 83 day test period. Degradation from 2-24 h (A) was 97 x 10^6 and 68 x 10^6 mg $mm^{-2}h^{-1}$ for

dH_2O and PBS, respectively; an increase in dH_2O by a factor of 1.43. The pH measurements indicated that the pH of the PBS solution was stable in the range 7.27-7.40 throughout testing. The pH of dH_2O was found to be between 6.77-7.02.

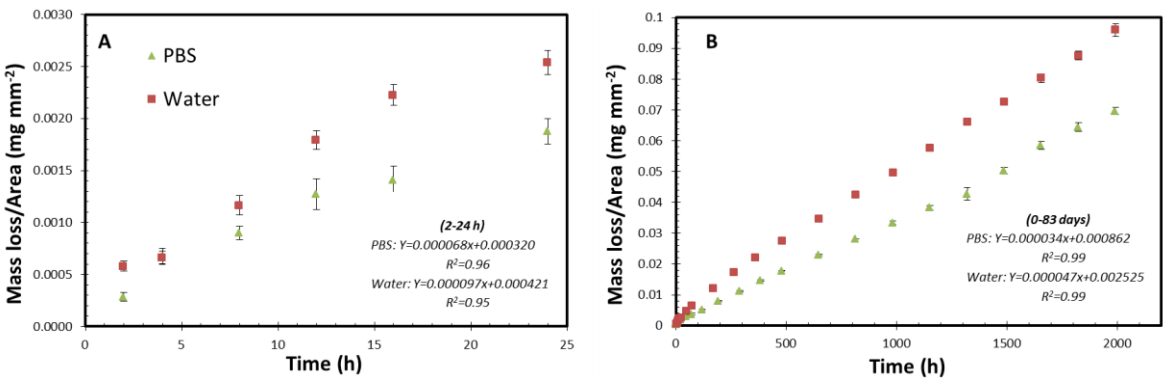

Figure 2: Degradation of melt quenched PBG C2: P40 in PBS and dH_2O. (A) Data up to 24 h. and (B) Full degradation period of 0-83 days.

3.3 Degradation of Glass Coatings in dH_2O

The degradation profiles of the two deposited coating compositions C1: P28, C2: P40 in dH_2O up to 24 h are shown in *Figure 3A* whilst *Figure 4A* shows the coating compositional variation of C2: P40.

Degradation rates revealed a linear profile between 2 h and 24 h as 50 x 10^6 and 210 x10^6 mg mm^{-2} h^{-1} for C1: P28 and C2: P40 respectively. Comparative mass losses at 2 h for C1: P28, and C2: P40 were 0.0014 and 0.0038 and mg mm^{-2} respectively. This indicated an increased solubility for both compositions during the first 2 h and also that C2: P40 degraded ≈4.2 x faster than C1: P28 *(see Figure 3A*).

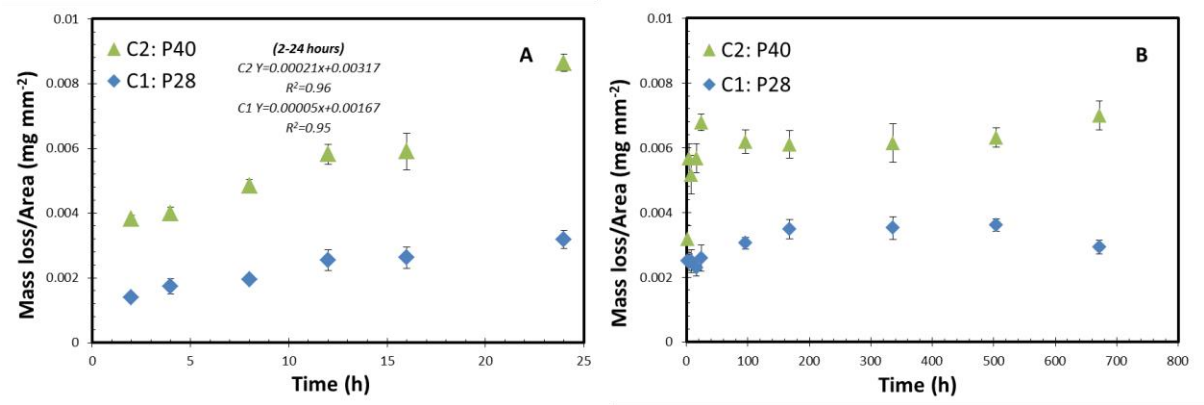

Figure 3: (A) Degradation of C1: P28 and C2: P40 on Ti6Al4V in dH_2O. (B) Degradation of C1: P28 and C2: P40 on Ti6Al4V in PBS.

The compositions C1 and C2 immersed in PBS, showed initial coating degradation followed by stabilisation within 24 h, after which no further mass loss was observed over the 28 day period (*Figure 3B*). The compositional changes of C2: P40 were followed up to 21 days, as determined by EDX (see *Figure 4B*) which showed compositional changes in the first 24 h. This profile could have possibly been associated with formation of a precipitate. The composition appeared to be stable by 24 hours.

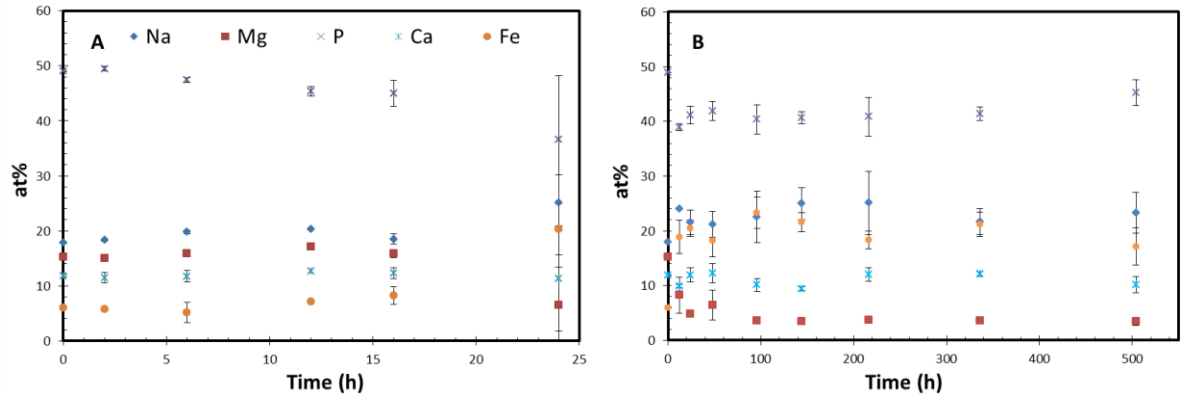

Figure 4: (A) EDX analysis of C2: P40 during degradation in dH_2O indicating consistent composition within the coating, suggestive of surface degradation. (B) Composition on the surface of C2: P40 at time points 0-21 days in PBS Solution indicating a variable composition in the first 24 hours.

3.4 FTIR of Coatings Pre and Post Degradation

The IR absorption results showed variations for C1: P28 and C2: P40 (*Figure 5A*). Analysis of B2: P40, which is similar in composition to C2: P40, showed similarities between the melt

quenched and sputtered glass. Absorption bands from C2: P40 found at 1096, 1034, 988, 885, 731 and 525 cm^{-1} were attributed to PO^- chain terminators, $(PO_3)^-$ asymmetric stretching chain ends, $(PO_3)^-$ symmetric stretching, P-O-P asymmetric stretching, P-O-P symmetric stretching and PO^- deformation modes respectively [35-38]. All stated IR absorption bands were found in B2: P40 and B1: P28 however in B1: P28 the band associated with PO^- chain terminators is represented by a shoulder than a peak. Similarly all bands were present in C1: P28 with the exception of 1034 at cm^{-1}, attributed to $(PO_3)^-$ symmetric stretching. In C1: P28 and B1: P28 distinct peaks associated with PO^- were present at 575 cm^{-1}. Variation in the positioning of the absorption band reflects slight compositional variation between C2: P40 and B2: P40 as shown in *Figure 5A*. Relative positioning of the absorption bands varied between compositions, as vibration frequency under excitation is dependent upon ionic bonds further down the covalent linkage. Slight shoulders may be a consequence of overlapping peak positions and variable intensities [35-38]. *Figure 5B* in comparison to (A) suggested no change in IR absorption properties following the 16 h degradation time points for coating C1: P28, or C2: P40.

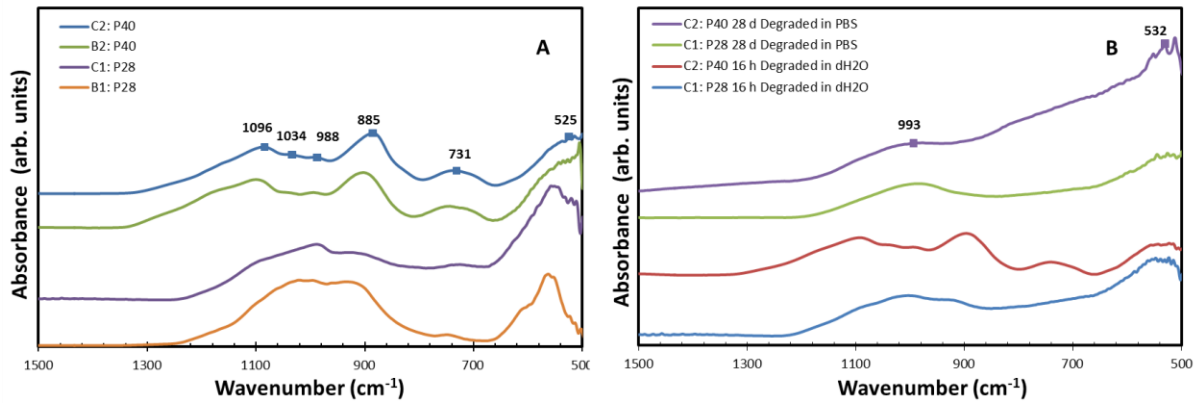

Figure 5: IR absorbance spectra of (A) bulk glass B1: P28, B2: P40, and as deposited coatings C1: P28 and C2: P40. (B) C1: P28 and C2: P40 16 h post degradation in dH_2O and 28 days post degradation in PBS of C1: P28 and C2: P40.

Following 28 d of degradation in PBS, FTIR *(Figure 5B)* absorbance at 993 cm^{-1} for C1: P28 and C2: P28 confirmed remaining bonds associated with $(PO_3)^-$ symmetric stretching. Peaks around 532 cm^{-1} indicate remaining PO^- deformation modes [35-38].

3.5 X-Ray Photoelectron Spectroscopy for Melt Quenched Rods Compared with Sputter Deposited Coatings

The XPS survey spectra confirmed the surface composition of coatings and bulk rods containing P, Mg, Ca, Na and Fe. High resolution scans showed the presence of adventitious carbon in the form of C-C, C-O-C and O-C=O bonds at their respective locations of 284.86, 286.61, 288.88 eV [39]. See *Table 4* for deconvolution of the high resolution spectra for all glass compositions tested suggested peaks associated with phosphate glass, notably, for B2: P40, two peaks within the O 1s corresponding to P-O-P bridges and (PO^- and P=O) non-bridging oxygen bonds at 531.72 and 533.44 eV respectively as suggested by Brow *et al* and Shih *et al* [36, 40]. B2: P40 showed deconvolution of the P 2P 3/2 and 1/2 high-resolution spectral peaks, specifically the P 2p 3/2 and P 2p 1/2 spin orbitals at 134.4 and 133.5 eV, attributed to $(P_2O_7)^{4-}$ and $(PO_4)^{3-}$ [41 42]. In contrast the surface of the coating C2: P40, was deconvoluted, containing peaks located at the P 2P 2/3 and 1/2 locations of 134.27 and 135.14 which were suggested to be attributed to metaphosphates $(PO_3)^-$ (see *Table 4*) [42 43].

The Q^n distribution (average number of bridging oxygens/ tetrahedral) on the surfaces of each glass coating composition as stated in *Table 4* for B2: P40 could be attributed to Q^0 and Q^1 orthophosphate and pyrophosphate linkages respectively and mainly Q^2 metaphosphates for C2: P40.

Comparison of BO to NBO linkages in melt quenched and sputter coated glass showed structural variations as manufactured, followed by similarity to melt quenched glass following 16 h degradation in dH_2O (*Table 4*).

Additionally, suggestions of metal phosphate bonds, PO^-, P-O-P bridges and oxides associated with ionic linkages for the alkali metals Na, Mg and Ca connected to the PO^- site support the presence of glass. High resolution spectra associated with Na 1s, Ca 2p, Mg 2s, Fe 2p supported oxidation states characteristic of the metal oxides for all XPS spectras.

Following 4 d of degradation in PBS the P 2P deconvolution was attributed to $(PO_3)^-$, in support of the FTIR results in *Figure 5B.* A notable increase from 5% to 23.7 % Na KLL following 4 d degradation in PBS of C2: P40 indicated a surface compositional increase in Na or possible precipitation of Na onto the surface.

Table 4: Deconvolution of the O 1s and P 2p to determine the ratio of Bridging to Non Bridging Oxygen's and states of phosphorus in the structure of C2: P40 Vs. B2: P40 surface. Ratios have been normalised to remove Na KLL from the peak deconvolution.

Glass Code	O 1s P-O-P Bridging (BO) (normalised)	O 1s PO^- and P=O Non Bridging (NBO) (normalised)	Na KLL (Overlapping O 1s)	P 2P 1/2 (eV)	P 2P 3/2 (eV)	Q^n Distribution
B2: P40 As Quenched	20.5	78.5	5.5	134.4	133.5 $(PO_4)^{3-}$ and $(P_2O_7)^{4-}$ [41 42]	Orthophosphate and Pyrophosphate and (Q^0 and Q^1) [40]
C2: P40 As Deposited	34.2	65.8	5.0	135.1	134.3 $(PO_3)^-$ [42]	Metaphosphate (Q^2) [40]
C2: P40 16 h In dH_2O	22.5	77.5	5.4	134.5	133.6 $(PO_4)^{3-}$ and $(P_2O_7)^{4-}$ [41 42]	Orthophosphate and Pyrophosphate and (Q^0 and Q^1) [40]
C2: P40 4 d In PBS	19.3	80.7	23.7	135.7	134.8 $(PO_3)^-$ [42]	Metaphosphate (Q^2) [40]

3.6 Scanning Electron Microscopy of Coating C2: P40 Degraded in dH_2O

Micrographs of C2: P40 at time points 0, 4, 16 and 24 h showed the development of pores from the surface through to the depth of the coating whilst degraded in dH_2O as shown in *Figure 6A, B, C and D* respectively. Void formation was observed to spread outwards from the centre of the pore until the coating was entirely degraded by the 48 h time points. Similar behaviour was observed on coatings deposited on roughened substrates as shown in the inserts for *Figure 7C vs. D* showing a coating view from above, similar to *Figure 6*. To investigate this

further, a cross section was milled through the pre and post degraded coatings via a FIB-SEM for both polished (*Figure 7A and B*) and sandblasted substrates (*C and D*). Observation of these corrosion pits appeared to suggest preferential sites for degradation, thus highlighting structural variability across the coating surfaces.

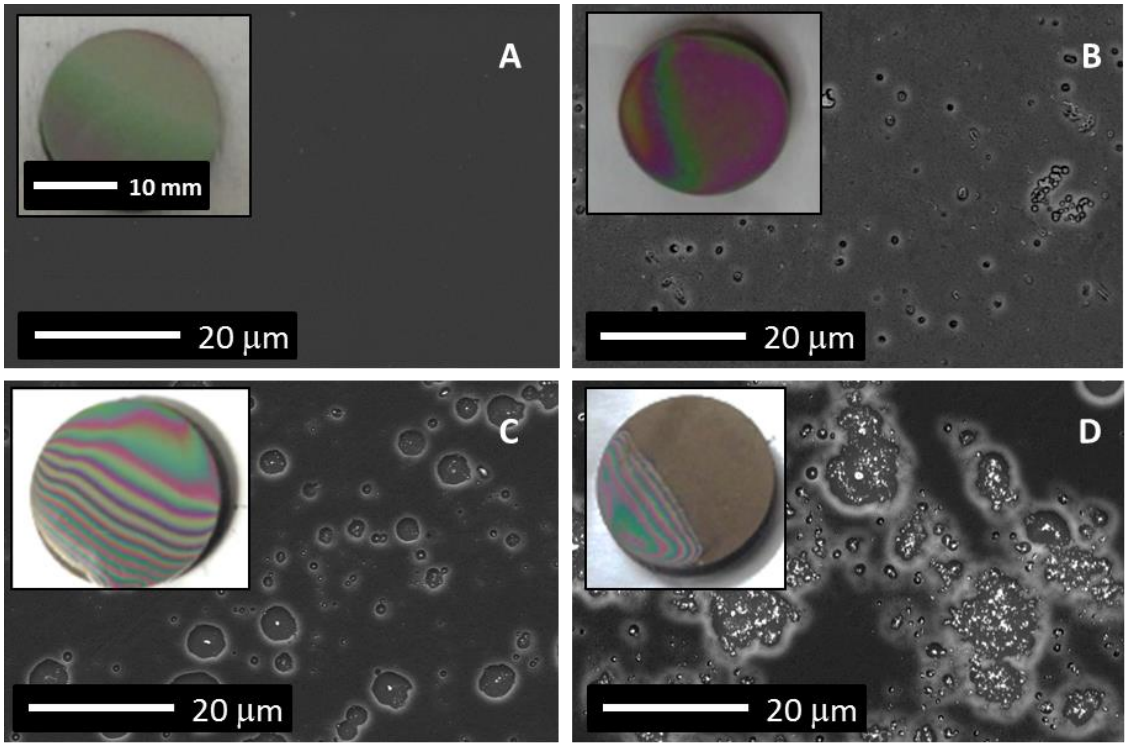

Figure 6: Complete coating degradation of phosphate glass on polished substrates. C2: P40 in dH_2O representing (A) coated and subsequent degradation for (B) 4 h, (C) 16h (D) 24 h.

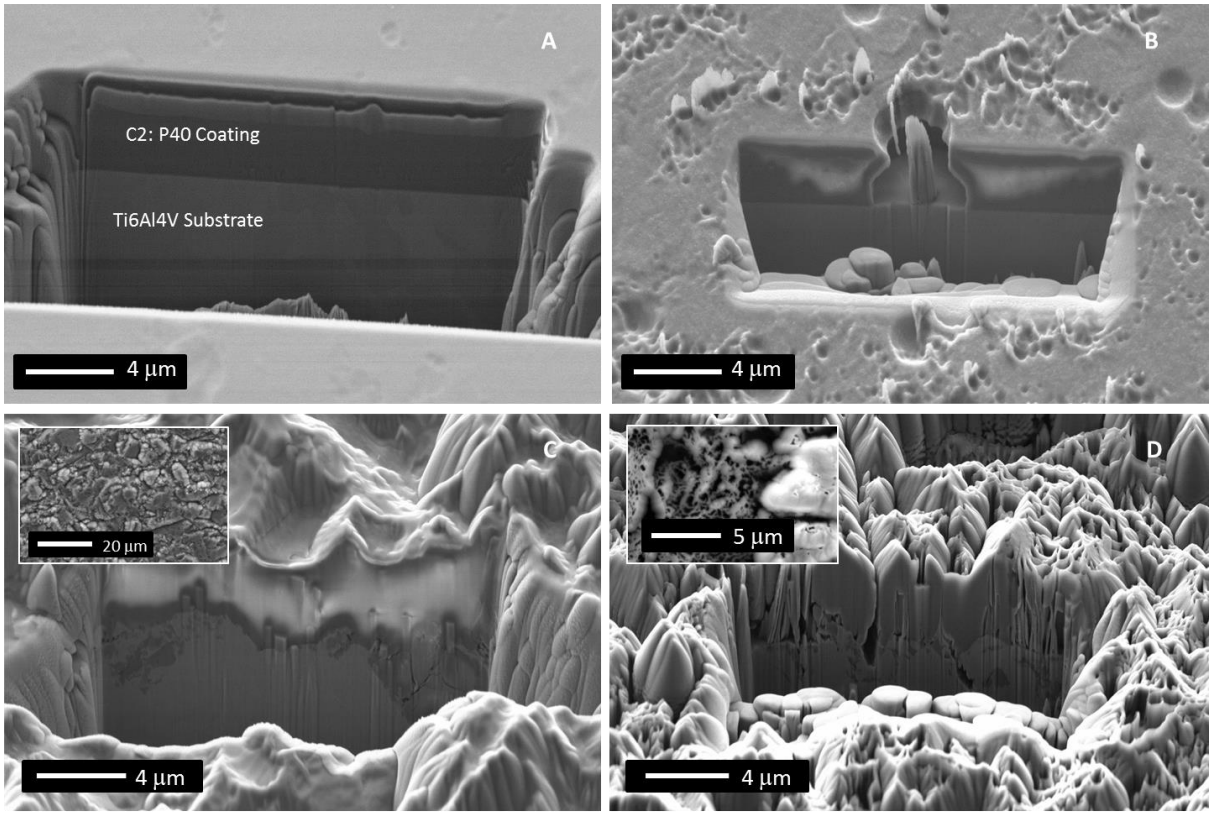

Figure 7: C2: P40 in dH_2O. (A) (Cross sectional FIB-SEM of an as deposited coating on a polished substrate. (B) Micrograph of a 16 h degraded coating, milled into a corrosion pit. (C and D) on sandblasted Ti6AL4V.

3.7 Scanning Electron Microscopy of Coating C2: P40 in PBS

Micrographs of the samples degraded in PBS up to 21 days suggested uneven coverage of particulates and remaining coating over the surface area of the sample as shown in *Figure 8A*, B and C for 4 h, 6 days and 21 days respectively. *Figure 8D* shows precipitates forming over a half coated specimen after 24 h whilst E and F show precipitation of coatings on sandblasted substrates after 48 h in solution at 2000x and 4000x respectively in contrast to micrographs for coatings of sandblasted substrates (E and F)

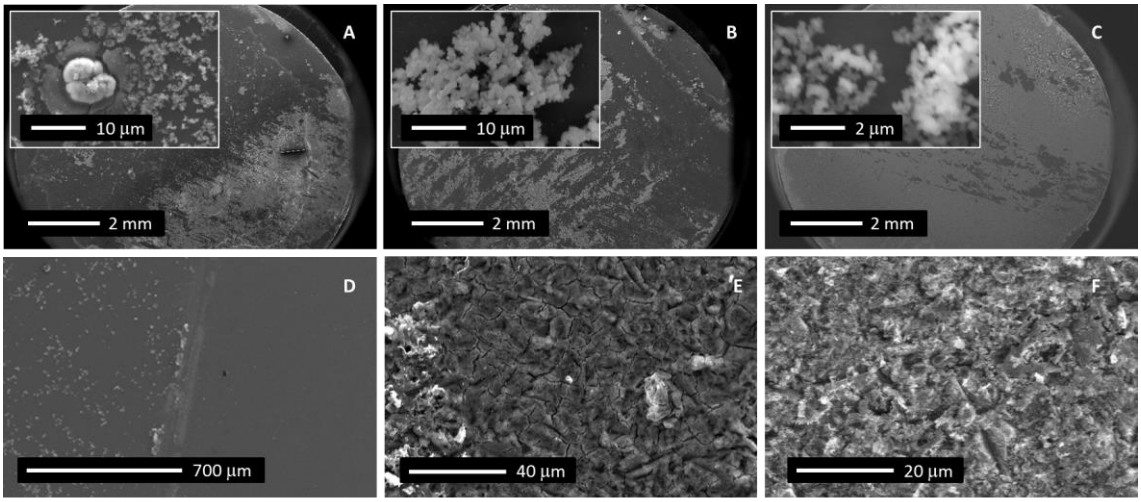

Figure 8: Degradation of C2: P40 phosphate glass on polished substrates in PBS representing (A) 4h, (B) 6 days, (C) 21 days degraded on sandblasted substrates. (D) Half coated samples (coated on left, uncoated on right) degraded in PBS for 24 h. (E) Precipitation on sandblasted surface after 48 h 2000x and (F) 4000x.

3.8 Contact Angle with dH_2O

Contact angle measurements (*Figure 9*) indicated a variation between bulk glass and the glass coating for the same mol% composition B2: P40 (24.8 ± 0.6 °) vs. C2: P40 (0-1% ± 0.50 °) (*Figure 9*). For both coating C1: P28 and C2: P40, the contact angle was between 0-1%, indicating complete hydrophilicity of the coating. In contrast sandblasted Ti6Al4V coated with C1: P28 had a contact angle of 44.6 ± 3.7° (n=5) for all contact angle experiments. Images of comparative contact angle for Ti6Al4V, B2: P40 and C2: P40 (insert in *Figure 9*). C1: P28 exhibited a similar profile to C2: P40. B1: P28 could not be manufactured similarly to C1: P28 due to crystallisation during melt quenching and therefore the contact angle was not compared. The hydrophilic nature as shown by contact angle correlates with the variable surface chemistries between B2: P40 and C2: P40 as shown by XPS (*Table 4*).

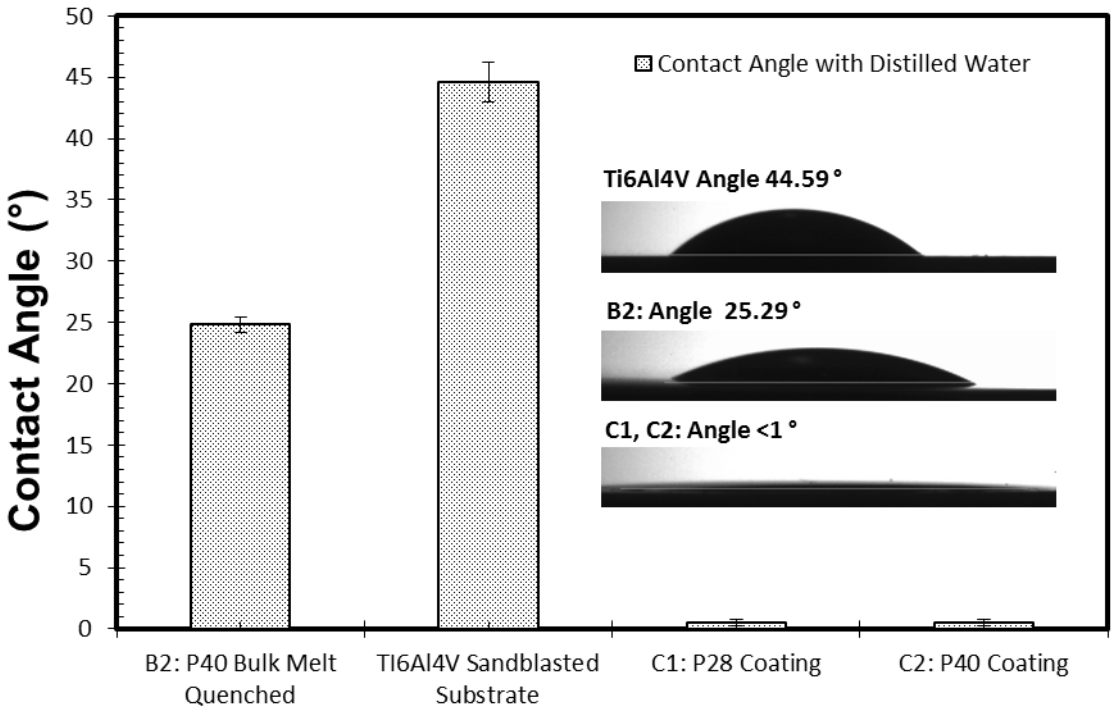

Figure 9: Contact angle of melt quenched and sputter coated glasses.

4. Discussion

Two bulk formulations B1: P28 and B2: P40 (see *Table 5*) were prepared by melt quenching and compared to coatings produced by magnetron sputtering using a glass target of a single formulation. EDX analyses confirmed that the compositions of the sputtered coatings C1: P28, C2: P40 were consistent with the bulk glass manufactured by melt quenching (B1: P28 and B2: P40) whilst XRD confirmed B2: P40 and C2: P40 to be amorphous (see *Figure 1A*). The FTIR results suggested structural similarities for B2: P40 and C2: P40 with identical IR absorption spectra's (*Figure 5A*). However, B1: P28 and C1: P28 showed variable IR absorption behaviour which probably resulted from differences in microstructure due to crystallisation of B1: P28 during the melt quenching process *(Figure 5A).*

Below a threshold limit of a network forming content, crystallisation may occur as seen in the case of B1: P28, for which the melt could not be quenched fast enough to maintain its amorphous disordered structure [44]. In contrast the near instantaneous atom-by-atom

condensation from magnetron sputtering to form a coating, enabled a glass/ceramic structure of C1: P28 composition to be formed containing a single crystal phase which was attributed to Lepidocrocite/FeOOH (*Figure 1A*). Ahmed *et al* reported surface crystals of $CaMgP_2O_7$ during rapid quenching of P_2O_5-40 CaO-25 Na_2O-5, MgO-30 mol% composition suggesting that the high divalent cation/phosphate ratio of 1.375 (or ratio of cross linking cations/phosphate = 2.75) was limiting the glass forming potential by conventional quenching for that glass system [45]. The calculated cation/phosphate ratio for the glasses produced here can be found in *Table 5*. B1: P28 maintained a ratio of 4.00, considerably beyond the suggested glass-forming window which led to crystallisation during melt quenching.

Table 5: Glass forming limits by cross-linking cation/phosphate ratios.

Composition (mol%)	Cross linking cation:phosphate ratio	Melt quenched structure
B1/C1: P28 Mg27 Ca20 Na19 Fe6	4.00	Bulk crystallisation
B2/C2 : P40 Mg24 Ca16 Na16 Fe4	2.30	Amorphous
P40 Ca25 Na5 Mg30	2.75 [45]	Surface crystallisation

pH

Bunker *et al* showed degradation of phosphate glasses to be highly pH dependent, with increased degradation at lower pH resulting from the higher level of free H^+ in solution. H_2O molecules attack the polymer-like P-O-P chains, which break and form OH-P-OH bonds [30]. Subsequent release of H^+ during dissolution could also lead to autocatalysis. Ahmed *et al* and Abou Neel *et al* suggested that this dissolution of the chains to form such bonds in solution led to formation of phosphoric acid, lowering the pH of the media [7, 46].

The solutions were changed periodically (twice per week) and the pH readings were obtained throughout the degradation period in PBS and dH_2O. During the degradation of B2: P40, pH values remained between 7.27-7.40 and 6.77-7.02 for PBS and dH_2O respectively. The pH

results for C1: P28 and C2: P40 degradation remained between 7.30 and 7.48 following precipitate formation. The pH values were not obtained for degradation of coatings in dH_2O as the low conductivity due to the lack of ions in solution led to continuous drifting of measurements. This inability indicated that the solution did not at any point become saturated. In contrast, degraded bulk glasses released sufficient ions over 24 h in the solution which enabled stable pH readings.

Degradation

According to Bunker *et al* and Gao *et al*, the degradation of phosphate glasses in water occurs in three stages; the acid/base reaction in which H_2O atoms react with network modifying cations to form H^+ ions in solution and free cations, interchanged with terminal OH^- species. Secondly cleavage of the P-O-P bonds occurs followed by the third stage of polymer like disentanglement [30-31]. The degradation profile of $t^{1/2}$ was used to describe an initial exponential degradation profile, described by Bunker *et al* as the initial diffusion of solution or hydration of the surface layer prior to hydrolysis and polymeric disentanglement. The partially hydrated layer beneath is then exposed as the surface layer [30].

The formed B2: P40 bulk glass rods were degraded in dH_2O over a period of 83 Days. The coatings C1: P28 and C2: P40 were degraded until the entire coating was dissolved with most of the degradation occurring within 24h (*Figure 3A*, and *7A-D*).

Preliminary dissolution of the coating compositions C1: P28 and C2: P40 showed an exponential degradation profile, defined by Bunker *et al* as the ($t^{1/2}$) phase, followed by a decline towards linear dissolution (*Figure 3A*). The degradation of the coatings in distilled water appeared to follow the degradation trend observed for the bulk glass compositions reported in literature. The two coatings, C1: P28 and C2: P40, exhibited a steeper initial solubility in comparison to melt quenched B2: P40 (*Figure 2A*) and continued to degrade

exponentially in the first 2 h, approaching the linear profile thereafter. The variation between sample solubility in the exponential phase may be attributed to chelating modifying ions and the depth of water penetration into the sample [31 30].

The hydrophilic nature of the deposited phosphate glass coatings as indicated by a completely wetted surface for all coatings, compared to 24.8° for B2: P40 (*Figure 9*), suggested faster hydration through the depth of the coating layer led to super hydration. The hydrated layer cannot expand beyond the depth of the substrate and thereafter led to lateral dissolution as suggested by the cross sectional FIB-SEM micrograph of the degraded coatings (*Figure 7B*), (*Figure 7D*), SEM observation of coating C2: P40 degraded in dH_2O at time points 4-24 h showed surface voids expanding with time, until the coating was entirely eroded by the 48th h in solution (*Figure 6*) Similar voids were also apparent on the sand blasted substrates; however the spread of voids was discontinuous due to the substrate roughness (C), *(Figure 7D*). Haque *et al* reported the peeling or "pitting corrosion" of P_2O_5-40 CaO-25 Na_2O-5, MgO-30 mol% fibres following 8 h degradation in water [47]. Abou Neel *et al* experienced a similar peeling effect for iron containing fibres [7]. This peeling effect in fibres was suggested to be due to the differential hydration between surface and bulk layers leading to tensile forces and subsequent cracking [48].

Dissolution in a thin-film glass or a glass surface layer may be most dependent upon the ability of the media to diffuse, increased by the concentration of P-O-P linkages in the surface and sub-surface layers. The most significant structural variation was observed in C2: P40 compared to B2: P40 which suggested a ratio of P-O-P to PO^- of 34.2% to 65.8% compared with 20.5% to 78.5% respectively. Deconvolution of the P 2P on the surface C2: P40 suggested the presence of more soluble (Q^2) $(PO_3)^-$ metaphosphate structures (*Table 4*) [40]; further supported by the high concentration of P-O-P bonding in the coatings. This would. therefore explain the increase in hydrophilicity of the coatings compared to the melt

quenched glass surfaces, which were found to contain $(P_2O_7)^{4-}$ and $(PO_4)^{3-}$, (Q^1 and Q^0) structures respectively [40-41 42]. This could also explain the increased degradation rate over the initial 24 h, and the initial rapid $t^{1/2}$ phase in the first 2 h. Abou Neel *et al* showed variation in polarity from contact angle measurements with water which was suggested to be due to P-O-P bonding in the wetted surface layer [7].

Gao *et al* suggested a model relating the distance of hydration into a glass surface, following initial exposure in solution. It was suggested that the rate of hydration was fastest during initial exposure and water diffusion through the layer decreased with thickness. This was followed by a steady state hydration rate during which degradation becomes linear [31].

XPS results following 16 h of degradation of C2: P40 in dH_2O showed P-O-P to PO^- ratio for coatings of 22.5% to 77.5% and presence of $(P_2O_7)^{4-}$ and $(PO_4)^{3-}$ (*Table 4*) similar to B2: P40 melt quenched suggesting that beyond the surface layer C2: P40 and B2: P40 may be structurally equivalent.

The surface variation analysed between melt quenched and sputtered coatings may relate to the surface sputtering process causing structural changes on the surface of the coating; characteristic of etching [49]. This suggests that ion bombardment of the coating surface led to the highly soluble phosphate structure observed and to preferential sites for dissolution.

Following the $t^{1/2}$ phase, the coating compositions tested exhibited linear dissolution rates of between 2-24 h of 50 x 10^6 and 210 x 10^6 mg mm^{-2} h^{-1} for C1: P28 and C2: P40 respectively (*Figure 3A*). Comparative dissolution rates are primarily related to the network connectivity of the glass structure are therefore dominated by the covalently bonded (P-O-P) structure and by ionic cross linking from the inclusion of cations such as magnesium, calcium, sodium and iron present in the three compositions tested [1, 7, 30, 45, 50].

Iron incorporation as a Fe-O-P linkage is known to result in lower solubility, leading to the C1: P28 sample being least soluble [7, 51]. Identification of broad diffraction peak at 38° (2θ) was observed for coating C1: P28 indicating partial crystallisation with a Lepidocrocite phase to form a glass ceramic during magnetron sputtering (*Figure 1A*).

Comparison of degradation in dH_2O of B2: P40 and C2: P40 showed linear degradation profiles, over the initial 2-24 h which was 2.06 times faster in the coating than its melt quenched counterpart. Degradation rates are influenced by processing routes, such that thermally annealed glasses degrade at slower rates compared to their melt quenched counterparts [47, 52-53]. Magnetron sputtering produces instantaneously quenched coatings upon a substrate, forming residual tensile stresses within the atomic layers, which may therefore account for higher degradation rates within the glass. Cozien-Cazuc *et al* showed annealing at 5 °C below the T_g for fibres, allowing the structure to reorientate to its more thermodynamically stable position and relieving internal stresses reduced dissolution by half [52-53].

Degradation of coatings in PBS showed precipitate formation. Following submersion degradation was halted *Figure 3B*, firstly for C1: P28, followed by the C2: P40 composition indicating that variation in initial ion release may have been related to the formation of a diffusion inhibiting precipitate layer above the remaining glass. *Figure 8* shows time points up to 21 days during which formation of a layer was observed on both polished and sandblasted substrates.

Comparison of coatings on polished and sand blasted substrates showed similar degradation rates as expected however delamination was observed on polished samples whilst elemental mapping for phosphorous on a degraded coating in PBS combined with uniform precipitation indicated complete coverage on the sand blasted (Ra = 0.788 μm) substrates.

Particulate formation was first apparent after 4 h in PBS (*Figure 8A*). Pitting corrosion as seen in dH_2O was observed. At all-time points beyond 4 h dissolution characteristics were no longer apparent in the form of pitting, leading to the likelihood that the rate of precipitate formation exceeded the dissolution reaction between 4 and 12 h in solution (*Figure 8A* and *B*). Varila *et al* attempted to quantify dissolution through mass changes, however, this proved problematic as dissolution was coupled with Ca:P formation on the surface, thus the net mass change was equated as dissolution+layer formation. In PBS the well-known Bioglass 45S5 revealed a net mass change of less than 0.2% over the 2 week test period. This mass change was suggested to be the result of counteracting reactions of dissolution and layer formation and therefore mass change was not indicative of the dissolution [54].

In the first 24 h a dissolution inhibiting diffusion barrier had formed. By 12 h the initial glass composition had changed. The compositional changes as determined by EDX, stabilised by 24 h *(Figure 4B)*. Submersion in PBS up to 21 days indicated a fully stable coating layer covered with particles. XRD data for C1: P28 and C2: P28, 28 days post degradation suggested amorphous precipitation with no additional crystalline phases beyond those detected in the substrate or the phase of FeOOH found in C1: P28 *(Figure 1B)*. The FTIR absorption spectra 28 days post submersion showed remaining bonds associated with $(PO_3)^-$ and PO^- deformation modes supported structural changes associated with formation of stable precipitation (*Figure 5B*).

Furthermore, XPS deconvolution of the P 2P supported the FTIR and showed surface structural changes (*Table 4*) attributed to $(PO_3)^-$, forming a (Q^2 structure) [40, 42]. Quantification was conducted in at% to reflect potential changes in oxidation states associated with the precipitation. Variation from the original composition of *C2:* P49 Na18 Mg15 Ca12 Fe6 at% to P41 Na22 Mg4 Ca12 Fe21 at% as analysed by EDX showed an insignificant change from 0.25 bulk Ca:P ratio to 0.29. The changes indicated a large increase in Fe from 6-21 at%, and

an increase in Na from 18 to 22 at% respectively. No further signs of compositional changes were observed beyond 12 h. This stabilised layer composition suggests a partially dissolved phosphate glass coating layer, on which a stable precipitated layer formed.

Based on the XPS compositional analysis, 4 days post degradation in PBS an increase in Na from 4.1% pre degradation to 30.6% post PBS degradation and an increase in Fe from 1.3% to 2.9% suggested that the formed precipitation may be a Sodium Iron Metaphosphate; however further analysis using a more precise method to analyse the composition will be necessary to isolate and identify the precipitation from remaining glass and the substrate. The formation of a calcium phosphate (Ca:P) apatite layer in phosphate containing saline solutions [34, 55-58] has often been reported. For example Bioglass 45S5 and two other silicate based glasses with SiO_2 content of 53 wt% and 68 wt% were submerged in SBF, Tri-buffer solution (TRIS), PBS and osteoblast medium for up to two weeks to observe their surface reactions and potential in vitro bioactivity [57]. In TRIS, HA formation was observed during dissolution; however, as the layer formed further dissolution was inhibited as a "diffusion barrier" formed. The calcium ions released in PBS led to rapid formation of a Ca:P layer due to high concentrations of phosphates in solution which similarly prevented further dissolution through the newly formed diffusion barrier [57].

Yamamoto *et al* suggested that glass compositions containing magnesium were shown to be less efficient in the precipitation of HA [56]. A. Tas *et al* suggested that Mg functions as a crystallisation inhibitor forming X-Ray amorphous precipitants; a finding which could be linked to the stability of the precipitation formed from the glass C1: P28 and C2: P40, which appeared to be X-Ray amorphous following XRD [34].

A review by Cuneyt Tas *et al* concluded that precipitation layers could be biomimetically synthesised at (37°C, pH =7.4) in a range of aqueous saline solutions which specifically

contained similar ionic concentrations as extracellular fluid [34]. The particles formed in DMEM solution were similar in morphology to ones observed here and were found to be X-Ray amorphous. Coverage of precipitation on an optical glass slide submerged in media was reported to increase and stabilise by 48 h [34, 55].

Degradation of thin sputtered PBG coatings exhibited unique behaviour as compared to their melt quenched counterparts, attributed to variation in surface structure which consequently caused accelerated hydration. Early indications are that sputtered coatings exhibit potential for controlled degradation at an implant site whilst showing the additional possibility of forming favourable precipitation layers, which could show future benefits for osseointegration. A desirable outcome may be the potential formation of a stable Ca/P layer, similar in composition to HA. Ultimately the flexibility for various ion inclusions in PBG may allow for the stratified design of therapeutic coatings.

5.0 Conclusions

RF Magnetron sputtered phosphate glass coatings on Ti6Al4V substrates were observed to fully degrade in distilled water. The initial solubility or steepness of the $t^{1/2}$ phase for glass coatings exceeded that of melt quenched glasses, and was attributed to variable surface chemistries such that there were 34.2% P-O-P linkages at the surface of the coatings as compared to the 20.5% in melt quenched glass as shown by XPS. This may have been related to continuous surface etching during the sputtering process. The degradation rate of coatings from 2-24 h was shown to increase by a factor of 2.06 over melt quenched glasses, due to the variation in thermal history between melt quenched and sputter coated glasses. All analysis of C2: P40 sputter coated and B2: P40 melt quenched glass via FTIR and XPS (following removal of the surface layer) suggested structural equivalence.

Coatings of 2.67 μm in C2: P40 showed pitting corrosion associated with preferential hydration and degradation, which led to lateral dissolution. Coatings on sandblasted substrates exhibited greater stability such that no peel off was shown, although discontinuous pitting corrosion was present. This was visually observed via FIB-SEM cross sectional milling.

The composition C1: P28 was sputtered as a glass ceramic containing a single crystalline phase whilst the melt quenched glass B1: P28 was highly crystalline; indicating near infinite quenching rate, amorphous compositions, unseen by melt quenching could be formed as a glass or at the lower P_2O_5 extremities; a glass/ceramic.

The coatings degraded in PBS precipitated a stable precipitant within 24 h. Dissolution in the $t^{1/2}$ was observed until the precipitation reaction exceeded dissolution. Over a 21 day period no variation in the precipitant characteristics were noticed beyond stable formation. The precipitation may have inhibited further glass degradation as EDX analysis indicated the presence of remaining glass beneath the precipitation. The variation in surface coverage of the precipitation indicated poor adhesion on polished Ti6Al4V samples.

Acknowledgments

This work was funded through MeDe Innovation, the EPSRC Centre for Innovative Manufacturing in Medical Devices, under grant number EP/K029592/1.

References

(1) Neel, E. A. A.; Pickup, D. M.; Valappil, S. P.; Newport, R. J.; Knowles, J. C., Bioactive Functional Materials: a Perspective on Phosphate-Based Glasses. *J. Mater. Chem.* **2009,** *19* (6), 690-701.
(2) Ahmed, I.; Ready, D.; Wilson, M.; Knowles, J. C., Antimicrobial Effect of Silver-Doped Phosphate-Based Glasses. *J. Biomed. Mater. Res. A* **2006,** *79* (3), 618-26.
(3) Knowles, J. C., Phosphate Based Glasses for Biomedical Applications. *J. Mater. Chem.* **2003,** *13* (10), 2395-2401.

(4) Liu, X. L.; Grant, D. M.; Parsons, A. J.; Harper, L. T.; Rudd, C. D.; Ahmed, I., Magnesium Coated Bioresorbable Phosphate Glass Fibres: Investigation of the Interface Between Fibre and Polyester Matrices. *BioMed Res. Int.* **2013,** *13*.
(5) Sharmin, N.; Hasan, M. S.; Parsons, A. J.; Furniss, D.; Scotchford, C. A.; Ahmed, I.; Rudd, C. D., Effect of Boron Addition on the Thermal, Degradation, and Cytocompatibility Properties of Phosphate-Based Glasses. *BioMed Res. Int.* **2013,** *2013*, 12.
(6) Neel, E. A.; Ahmed, I.; Pratten, J.; Nazhat, S. N.; Knowles, J. C., Characterisation of Antibacterial Copper Releasing Degradable Phosphate Glass Fibres. *Biomaterials* **2005,** *26* (15), 2247-54.
(7) Neel, E. A.; Ahmed, I.; Blaker, J.; Bismarck, A.; Boccaccini, A.; Lewis, M.; Nazhat, S.; Knowles, J., Effect of Iron on the Surface, Degradation and Ion Release Properties of Phosphate-Based Glass Fibres. *Acta Biomater.* **2005,** *1* (5), 553-563.
(8) Ahmed, I.; Jones, I. A.; Parsons, A. J.; Bernard, J.; Farmer, J.; Scotchford, C. A.; Walker, G. S.; Rudd, C. D., Composites for Bone Repair: Phosphate Glass Fibre Reinforced PLA with Varying Fibre Architecture. *J. Mater. Sci. Mater. Med.* **2011,** *22* (8), 1825-34.
(9) Ahmed, I.; Collins, C. A.; Lewis, M. P.; Olsen, I.; Knowles, J. C., Processing, Characterisation and Biocompatibility of Iron-Phosphate Glass Fibres for Tissue Engineering. *Biomaterials* **2004,** *25* (16), 3223-3232.
(10) Hasan, M. S.; Ahmed, I.; Parson, A. J.; Walker, G. S.; Scotchford, C. A., Material Characterisation and Cytocompatibility Assessment of Quinternary Phosphate Glasses. *J. Mater. Sci. - Mater. Med.* **2012,** *23* (10), 2531-2541.
(11) Kasuga, T.; Fujimoto, T.; Hosoi, Y.; Nogami, M., Calcium Phosphate Invert Glasses and Glass-Ceramics with Apatite-Forming Ability. *Bioceramics 15* **2003,** *240-2*, 265-268.
(12) Hench, L. L., The Story of Bioglass. *J. Mater. Sci. Mater. Med.* **2006,** *17* (11), 967-78.
(13) Massera, J.; Mayran, M.; Rocherulle, J.; Hupa, L., Crystallization Behavior of Phosphate Glasses and its Impact on the Glasses' Bioactivity. *JMatS* **2015,** *50* (8), 3091-3102.
(14) Kim, H. W.; Lee, E. J.; Jun, I. K.; Kim, H. E., On the Feasibility of Phosphate Glass and Hydroxyapatite Engineered Coating on Titanium. *Journal of Biomedical Materials Research Part A* **2005,** *75* (3), 656-667.
(15) Sun, L.; Berndt, C. C.; Gross, K. A.; Kucuk, A., Material Fundamentals and Clinical Performance of Plasma-Sprayed Hydroxyapatite Coatings: a Review. *J. Biomed. Mater. Res.* **2001,** *58* (5), 570-92.
(16) Yamashita, K.; Arashi, T.; Kitagaki, K.; Yamada, S.; Umegaki, T.; Ogawa, K., Preparation of Apatite Thin Films Through RF-Sputtering from Calcium Phosphate Glasses. *J. Am. Ceram. Soc.* **1994,** *77* (9), 2401-2407.
(17) Lo, W. J.; Grant, D. M., Hydroxyapatite thin films deposited onto uncoated and (Ti,Al, V)N-coated Ti alloys. *J. Biomed. Mater. Res.* **1999,** *46* (3), 408-17.
(18) Wolke, J. G.; van Dijk, K.; Schaeken, H. G.; de Groot, K.; Jansen, J. A., Study of the Surface Characteristics of Magnetron-Sputter Calcium Phosphate Coatings. *J. Biomed. Mater. Res.* **1994,** *28* (12), 1477-84.
(19) Boyd, A. R.; O'Kane, C.; Meenan, B. J., Control of Calcium Phosphate Thin Film Stoichiometry Using Multi-Target Sputter Deposition. *Surf. Coat. Technol.* **2013,** *233* (0), 131-139.
(20) Mardare, C. C.; Mardare, A. I.; Fernandes, J. R. F.; Joanni, E.; Pina, S. C. A.; Fernandes, M. H. V.; Correia, R. N., Deposition of Bioactive Glass-Ceramic Thin-Films by RF Magnetron Sputtering. *J. Eur. Ceram. Soc.* **2003,** *23* (7), 1027-1030.
(21) Stan, G. E.; Popescu, A. C.; Mihailescu, I. N.; Marcov, D. A.; Mustata, R. C.; Sima, L. E.; Petrescu, S. M.; Ianculescu, A. R.; Trusca, R.; Morosanu, C. O., On the Bioactivity of Adherent Bioglass Thin Films Synthesized by Magnetron Sputtering Techniques. *Thin Solid Films* **2010,** *518* (21), 5955-5964.
(22) Stan, G. E.; Pina, S.; Tulyaganov, D. U.; Ferreira, J. M.; Pasuk, I.; Morosanu, C. O., Biomineralization Capability of Adherent Bio-Glass Films Prepared by Magnetron Sputtering. *J. Mater. Sci. Mater. Med.* **2010,** *21* (4), 1047-55.

(23) Stan, G. E.; Morosanu, C. O.; Marcov, D. A.; Parsuk, I.; Miculescu, F.; Reumont, G., Effect of Anealing Upon the Structure and Adhesion Properties of Sputtered Bio-Glass/Titanium Coatings. *Appl. Surf. Sci.* **2009,** *255* (22), 9132-9138.
(24) Stan, G. E.; Marcov, D. A.; Pasuk, I.; Miculescu, F.; Pina, S.; Tulyaganov, D. U.; Ferreira, J. M. F., Bioactive Glass Thin Films Deposited by Magnetron Sputtering Technique: The Role of Working Pressure. *Appl. Surf. Sci.* **2010,** *256* (23), 7102-7110.
(25) Stan, G. E.; Bojin, D., Adherant Glass-Ceramic Thin Layer with Bioactive Potential Deposited by Magnetron Sputtering Techniques. *U.P.B Sci. Bull., Series B* **2010,** *72* (2), 187-196.
(26) Mistry, S.; Kundu, D.; Datta, S.; Basu, D., Effects of Bioactive Glass, Hydroxyapatite and Bioactive Glass–Hydroxyapatite Composite Graft Particles in the Treatment of Infrabony Defects. *Journal of Indian Society of Periodontology* **2012,** *16* (2), 241.
(27) Krishnan, V.; Lakshmi, T., Bioglass: A Novel Biocompatible Innovation. *Journal of advanced pharmaceutical technology & research* **2013,** *4* (2), 78.
(28) Stuart, B.; Gimeno-Fabra, M.; Segal, J.; Ahmed, I.; Grant, D. M., Preferential Sputtering in Phosphate Glass Systems for the Processing of Bioactive Coatings. *Thin Solid Films* **2015**.
(29) Ahmed, I.; Lewis, M.; Olsen, I.; Knowles, J. C., Phosphate Glasses for Tissue Engineering: Part 1. Processing and Characterisation of a Ternary-Based P2O5–CaO–Na2O Glass System. *Biomaterials* **2004,** *25* (3), 491-499.
(30) Bunker, B. C.; Arnold, G. W.; Wilder, J. A., Phosphate Glass Dissolution In Aqueous Solution. *J. Non-Cryst. Solids* **1984,** *64* (3), 291-316.
(31) Gao, H.; Tan, T.; Wang, D., Dissolution Mechanism and Release Kinetics of Phosphate Controlled Release Glasses in Aqueous Medium. *J Control Release* **2004,** *96* (1), 29-36.
(32) Kokubo, T.; Takadama, H., How Useful is SBF in Predicting in Vivo Bone Bioactivity? *Biomaterials* **2006,** *27* (15), 2907-2915.
(33) Avent, A. G.; Carpenter, C. N.; Smith, J. D.; Healy, D. M.; Gilchrist, T., The Dissolution of Silver-Sodium-Calcium-Phosphate Glasses for the Control of Urinary Tract Infections. *J. Non-Cryst. Solids* **2003,** *328* (1-3), 31-39.
(34) Tas, A. C., The Use of Physiological Solutions or Media in Calcium Phosphate Synthesis and Processing. *Acta Biomater.* **2014,** *10* (5), 1771-1792.
(35) Shih, P.; Ding, J.; Lee, S., 31P MAS-NMR and FTIR Analyses on the Structure of CuO-Containing Sodium Poly-and Meta-Phosphate Glasses. *Mater. Chem. Phys.* **2003,** *80* (2), 391-396.
(36) Shih, P. Y.; Yung, S. W.; Chin, T. S., FTIR and XPS Studies of P2O5-Na2O-CuO Glasses. *J. Non-Cryst. Solids* **1999,** *244* (2-3), 211-222.
(37) Omrani, R. O.; Kaoutar, A.; El Jazouli, A.; Krimi, S.; Khattech, I.; Jemal, M.; Videau, J. J.; Couzi, M., Structural and Thermochemical Properties of Sodium Magnesium Phosphate Glasses. *J. Alloys Compd.* **2015,** *632*, 766-771.
(38) Abid, M.; Et-Tabirou, M.; Hafid, M., Glass Forming Region, Ionic Conductivity and Infrared Spectroscopy of Vitreous Sodium Lead Mixed Phosphates. *Mater. Res. Bull.* **2001,** *36* (3), 407-421.
(39) Dementjev, A.; De Graaf, A.; Van de Sanden, M.; Maslakov, K.; Naumkin, A.; Serov, A., X-ray Photoelectron Spectroscopy Reference Data for Identification of the C 3 N 4 Phase in Carbon–Nitrogen Films. *Diamond Relat. Mater.* **2000,** *9* (11), 1904-1907.
(40) Brow, R. K., Review: the Structure of Simple Phosphate Glasses. *J. Non-Cryst. Solids* **2000,** *263* (1-4), 1-28.
(41) Puziy, A. M.; Poddubnaya, O. I.; Socha, R. P.; Gurgul, J.; Wisniewski, M., XPS and NMR Studies of Phosphoric Acid Activated Carbons. *Carbon* **2008,** *46* (15), 2113-2123.
(42) Wagner, C. D.; Naumkin, A. V.; Kraut-Vass, A.; Allison, J. W.; Powell, C. J.; Rumble Jr, J. R., *Nist Standard Reference Database*.
(43) Khattak, G.; Mekki, A.; Wenger, L., X-ray Photoelectron Spectroscopy (XPS) and Magnetic Susceptibility Studies of Vanadium Phosphate Glasses. *J. Non-Cryst. Solids* **2009,** *355* (43), 2148-2155.
(44) Tilley, R. J., *Understanding Solids: the Science of Materials*. John Wiley & Sons: **2004**.

(45) Ahmed, I.; Parsons, A.; Jones, A.; Walker, G.; Scotchford, C.; Rudd, C., Cytocompatibility and Effect of Increasing MgO Content in a Range of Quaternary Invert Phosphate-Based Glasses. *J. Biomater. Appl.* **2010,** *24* (6), 555-75.
(46) Ahmed, I.; Lewis, M.; Nazhat, S.; Knowles, J., Quantification of anion and cation release from a range of ternary phosphate-based glasses with fixed 45 mol% P2O5. *J. Biomater. Appl.* **2005,** *20* (1), 65-80.
(47) Haque, P.; Ahmed, I.; Parsons, A.; Felfel, R.; Walker, G.; Rudd, C., Degradation Properties and Microstructural Analysis of 40P2O5–24MgO–16CaO–16Na2O–4Fe2O3 Phosphate Glass Fibres. *J. Non-Cryst. Solids* **2013,** *375*, 99-109.
(48) Cozien-Cazuc, S.; Parsons, A.; Walker, G.; Jones, I.; Rudd, C., Effects of Aqueous Aging on the Mechanical Properties of P40Na20Ca16Mg24 Phosphate Glass Fibres. *J. Mater. Sci. - Mater. Electron.* **2008,** *43* (14), 4834-4839.
(49) Kester, D. J.; Messier, R., Micro-Effects of Resputtering Due to Negative-Ion Bombardment of Growing Thin-Films. *J. Mater. Res.* **1993,** *8* (8), 1938-1957.
(50) Christie, J. K.; Ainsworth, R. I.; Di Tommaso, D.; de Leeuw, N. H., Nanoscale Chains Control the Solubility of Phosphate Glasses for Biomedical Applications. *J. Phys. Chem. B* **2013,** *117* (36), 10652-7.
(51) Yu, X. Y.; Day, D. E.; Long, G. J.; Brow, R. K., Properties and Structure of Sodium-Iron Phosphate Glasses. *J. Non-Cryst. Solids* **1997,** *215* (1), 21-31.
(52) Cozien-Cazuc, S.; Parsons, A. J.; Walker, G. S.; Jones, I. A.; Rudd, C. D., Real-Time Dissolution of P40Na20Ca16Mg24 Phosphate Glass Fibers. *J. Non-Cryst. Solids* **2009,** *355* (50-51), 2514-2521.
(53) Choueka, J.; Charvet, J. L.; Alexander, H.; Oh, Y. H.; Joseph, G.; Blumenthal, N. C.; LaCourse, W. C., Effect of Annealing Temperature on the Degradation of Reinforcing Fibers for Absorbable Implants. *Journal of biomedical materials research* **1995,** *29* (11), 1309-1315.
(54) Han, L.; Okiji, T., Bioactivity Evaluation of Three Calcium Silicate-Based Endodontic Materials. *International endodontic journal* **2013,** *46* (9), 808-14.
(55) Cuneyt Tas, A., X-ray-Amorphous Calcium Phosphate (ACP) Synthesis in a Simple Biomineralization Medium. *Journal of Materials Chemistry B* **2013,** (35), 4511-4520.
(56) Yamamoto, S.; Nonami, T.; hase, H.; Kawamura, N., Fundamental Study on Apatite Precipititate Ability of CaO-MgO-SiO2 Compounders Employed Pseudo Body Solution of Application for Biomaterials. *JACS* **2012,** *48* (2), 180-184.
(57) Varila, L.; Fagerlund, S.; Lehtonen, T.; Tuominen, J.; Hupa, L., Surface Reactions of Bioactive Glasses in Buffered Solutions. *J. Eur. Ceram. Soc.* **2012,** *32* (11), 2757-2763.
(58) Fagerlund, S.; Hupa, L.; Hupa, M., Comparison of Reactions of Bioactive Glasses in Different Aqueous Solutions. *Advances in Bioceramics and Biotechnologies* **2010,** *218*, 101-113.

TOC "Graphic for manuscript"